PNAS Supplemental Information

Performance of flux-gradient method to measure GEM fluxes

The flux-gradient method quantifies GEM fluxes by measurement of concentrations at two heights above the canopy multiplied by the turbulent exchange coefficient. Detection of small GEM fluxes that exist over terrestrial ecosystems – often below 1 ng m^{-2} hr^{-1} (1) – is challenging because concentration differences measured between the two inlet heights are very small, a challenge amplified over forests due to high atmospheric turbulence which erodes concentration gradients. Figure S2A shows 30-minute resolution GEM concentration differences above the forest canopy (upper inlet at 31 m minus lower inlet at 24 m; note that negative values show deposition). High turbulence levels above this forest caused concentration differences to be very small with a median value of -0.0025 ng m^{-3}, a mean of -0.0027 ng m^{-3}, and an interquartile range (IQR) of -0.0142 ng m^{-3} to 0.0092 ng m^{-3}. The measured GEM concentration differences were about three to four times lower than those reported over lower-statured ecosystems such as grassland and a tundra (2). Measurements of individual pairs of GEM gradients were often below the detection limit of the GEM analyzer (about 0.05 ng m^{-3} based on 3 standard deviations of 5-minute resolution measurements). We estimate a median GEM flux detection limit of 34 ng m^{-2} hr^{-1} at 30-resolution based three standard deviations of paired fluxes using a daily-differencing method (see below), showing the need for time averaging such as using monthly hourly means and mediums (e.g., 60 flux data points) to delineate diel patterns and daily time averaging (e.g., 48 flux data points) for daily flux patterns.

In response, measurements required stringent quality assurance and control steps such as frequent filter exchange and line contamination and leak testing. An additional step that proved critical was frequent rotation of the two inlet sampling lines to test for presence of null gradients. Null gradients – systematic biases in concentrations between inlet lines – would result in a change or even reversal of concentration differences upon inlet rotation and yield differences in gradients before and after switching. Figure S2B shows cumulative values of measured GEM concentration differences with positive slopes indicating periods of emissions and negative slopes periods of deposition. Vertical green lines signify times when the two sampling inlets to measure GEM gradients were rotated for quality control purposes to test for presence of null gradients (i.e., line biases, see Method). The slopes of the cumulative graphs and statistical comparisons of gradient measurements one day prior to and after inlet rotation show that inlet rotation did not change fluxes or reverse flux directions.

To assess the statistical significance of measured GEM concentration differences, a cumulative periodogram (squared magnitude of the discrete Fourier transform, or power spectrum) was calculated (Figure S3A) which shows concentration differences to be statistically different from a white noise signal (Bartlett white-noise test: $P < 0.01$). This result confirms that at high frequencies, measured gradients were not based on random chance and represented an underlying exchange process that led to stratification of GEM in the lower boundary layer where GEM gradients were measured. Concentration differences also

showed strong autocorrelations (Figure S3B) over short lag times (e.g., minutes), which declined over several hours, and showed renewed peaks at subsequent daily lag times providing evidence of strong diel cycles in measured GEM concentration differences. Such autocorrelation patterns are visible and exceeding 95% confidence intervals for about two weeks, after which autocorrelations ceased.

In summary, frequency spectra and autocorrelations of measured GEM concentration differences showed underlying periodicity patterns, statistical differences from white noise signals. In addition, strong autocorrelations at short time lags and underlying diurnal patterns provide confidence that GEM concentration differences were highly structured in time and controlled by meteorological and physiological variables which imposed diel variability in ecosystem GEM fluxes.

Verification of flux-gradient method for CO_2 in comparison to Eddy Covariance fluxes

The flux-gradient method was chosen to quantify ecosystem-level GEM exchange as it is operable with low instrument time resolution (e.g. 2.5 to 5 minutes for GEM). Previous flux-gradient measurements at this forest site also were successfully conducted for carbonyl-sulfide (3), hydrogen (4), non-methane hydrocarbons (5, 6) and isoprene (7), including comparisons to Eddy Covariance (EC) fluxes (3) and disjunct EC fluxes (e.g., 8) showing good methods agreements. The flux-gradient method deployed above the forest was further verified at this site from June 12 to October 16, 2019 using comparisons of carbon dioxide (CO_2) flux-gradient method fluxes with fluxes measured by the EC technique, which is the most commonly used and preferred method to quantify trace gas fluxes when high time resolution detection is available (>1 Hz; (9)). CO_2 fluxes above the canopy using both the EC and flux-gradient method using the same implementation as for GEM described by (10) showed best agreement between methods with zero-displacement heights of 16.8 m, which is the value we used to process GEM fluxes and is very similar to values previously used at this forest site (10, 11). CO_2 fluxes calculated from the gradients reproduced diel cycles well and quantitatively agreed with EC fluxes (Figure S4). Daily CO_2 fluxes during the inter-comparison period amounted to 102 µmol m^{-2} s^{-1} using the EC method while the flux-gradient method resulted in 92 µmol m^{-2} s^{-1}, suggesting slight underestimation of fluxes using the flux-gradient method in comparison to the EC method. For forest floor CO_2 fluxes, also shown in Figure S4, no comparisons are available with an independent method. However, forest floor CO_2 exchange followed expected patterns of net emissions due to underlying forest floor and soil respiration processes.

Random error estimation and error propagation of GEM flux measurements

To quantify uncertainties in measured GEM fluxes, we conducted a random error analysis as described for other micrometeorological flux measurements by (12, 13). Tower methods generally do not allow for spatial replication, so time can be traded for space for error analysis using a “daily differencing” approach. In this approach, random errors are estimated based on variability of 30-minute time resolution fluxes taken on two successive days. Paired flux data of two days are formed only for equivalent environmental conditions for fluxes measured at the same time and under similar photosynthetic active radiation (within 75 µmol m^{-2} sec^{-1}), temperatures (within 3°C), and wind speeds (within 1 m sec^{-1}). A histogram of

measurement differences of all data pairs is shown in Figure S5A. Relative random errors are quantified using standard deviations of daily-differences GEM flux pairs versus the magnitude of fluxes (using flux bins of 10 ng m^{-2} hr^{-1}, Figure S5B). Slopes are fitted to separately for GEM fluxes below zero (i.e., deposition) and above zero (emissions), whereby slopes (Δstdev/Δmean) represent relative standard deviations for each bin of GEM flux measurements.

Subsequently, we assigned normal distribution function for each measured data point using its flux value as mean and the standard deviation calculated based on the regression line (i.e., intercept plus slope; Figure S5B). For each measurements, 500 random data points were assigned based on respective normal distribution. Figure S5C shows scatter plots for the first five randomly generated points against measured GEM flux showing examples of random errors associated with each flux GEM measurement point. Finally, cumulative sums of all 500 data columns generated were calculated for all 22,536 30-minuted GEM flux observations and 95% confidence intervals were calculated and graphed in figures and text in the manuscript where cumulative GEM sums are presented.

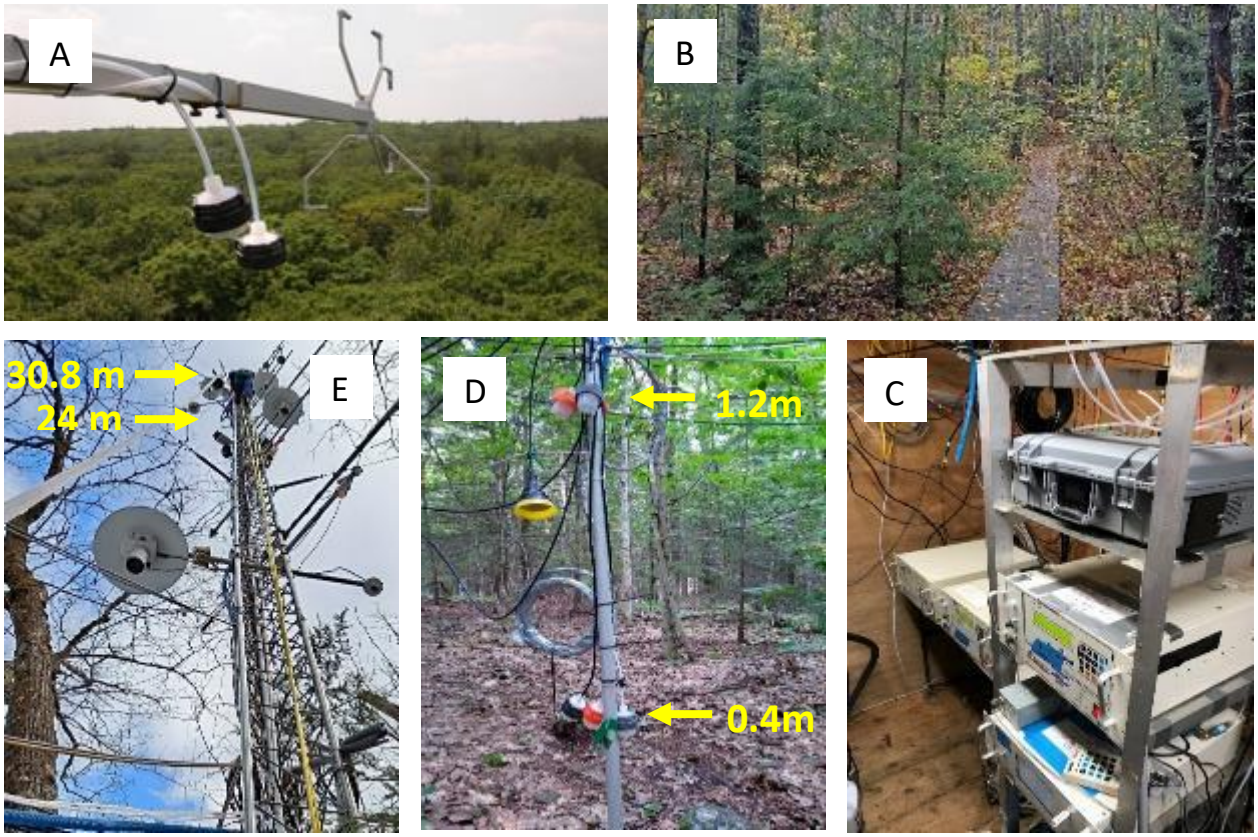

Figure S1. Measurement site at Harvard Forest. The study was performed at the Harvard Forest research station Environmental Monitoring Station (EMS) tower. Pictures from the top left (clock-wise) show: **A.** View over the deciduous forest canopy and of a sonic anemometer and upper inlets at the of the measurement tower; **B.** View of the forest floor with access pathway to the tower; **C.** Set-up GEM analyzers and a CO_2 analyzer inside a climate-controlled measurement laboratory; **D.** View of the forest floor gradients setup at 0.4 m and 1.2 m above the forest floor with inlets for GEM and CO_2 sampling; **E.** View of the large tower with flux-gradient inlets and instrumentations (24 m and 30.8 m above the ground) on top of the tower. Additional in-canopy instruments are used for other projects.

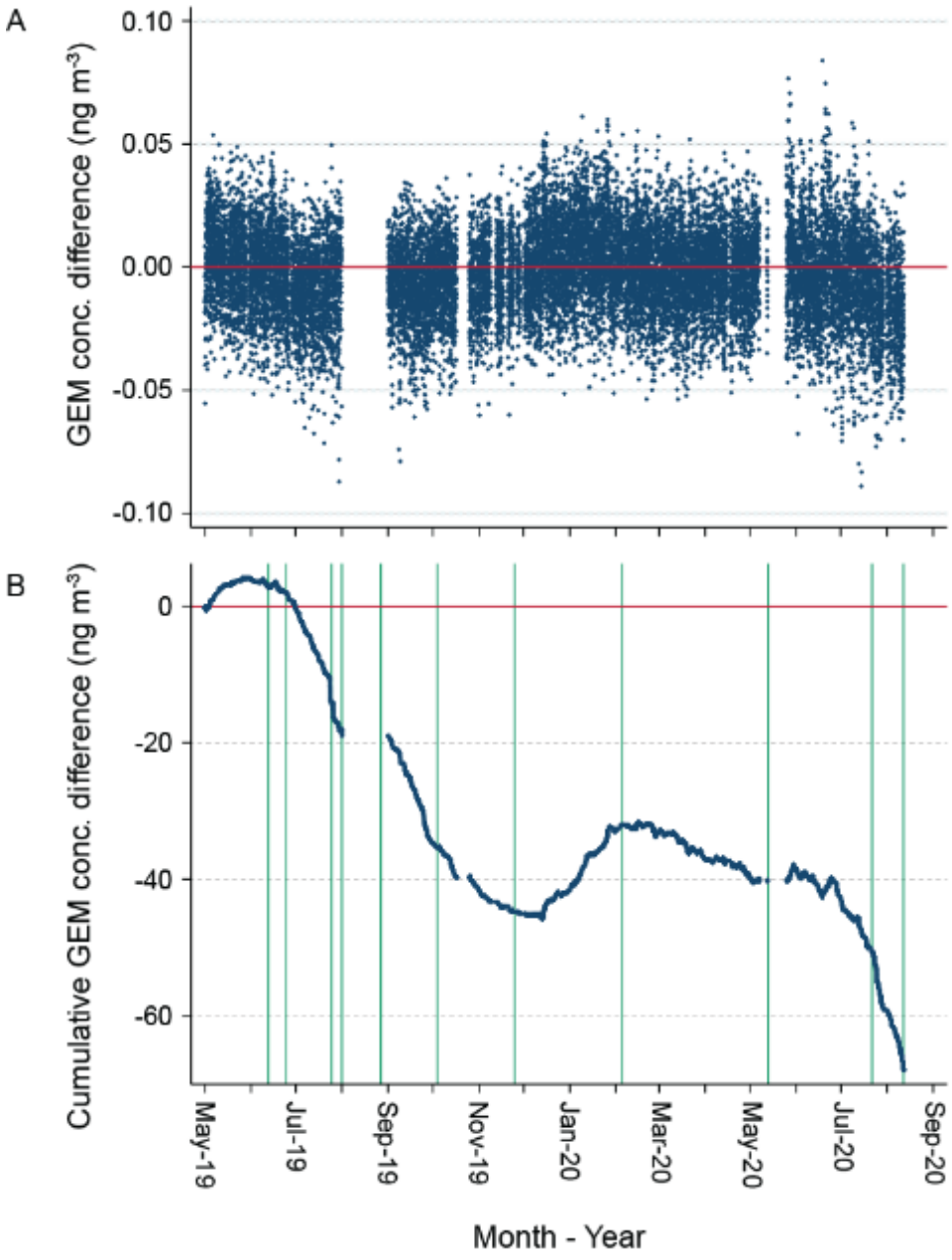

Figure S2A. 30-minute resolution GEM concentration differences (lower inlet – upper inlet concentrations) above the forest canopy. Positive values indicate emissions while negative values show deposition. **B.** Cumulative sum of 30-minute resolution concentration differences with slope direction indicating direction of fluxes (positive slopes emission, negative slopes deposition). Note that vertical green lines show times when inlet slopes were rotated which did not reverse flux directions and showed not significant difference in slope between one day of data prior to and after the line switch. Gaps in cumulative graph shows missing data due to power outages or other instrumentation failures (unlike the cumulative flux graph in Figure 1C, missing data was not interpolated).

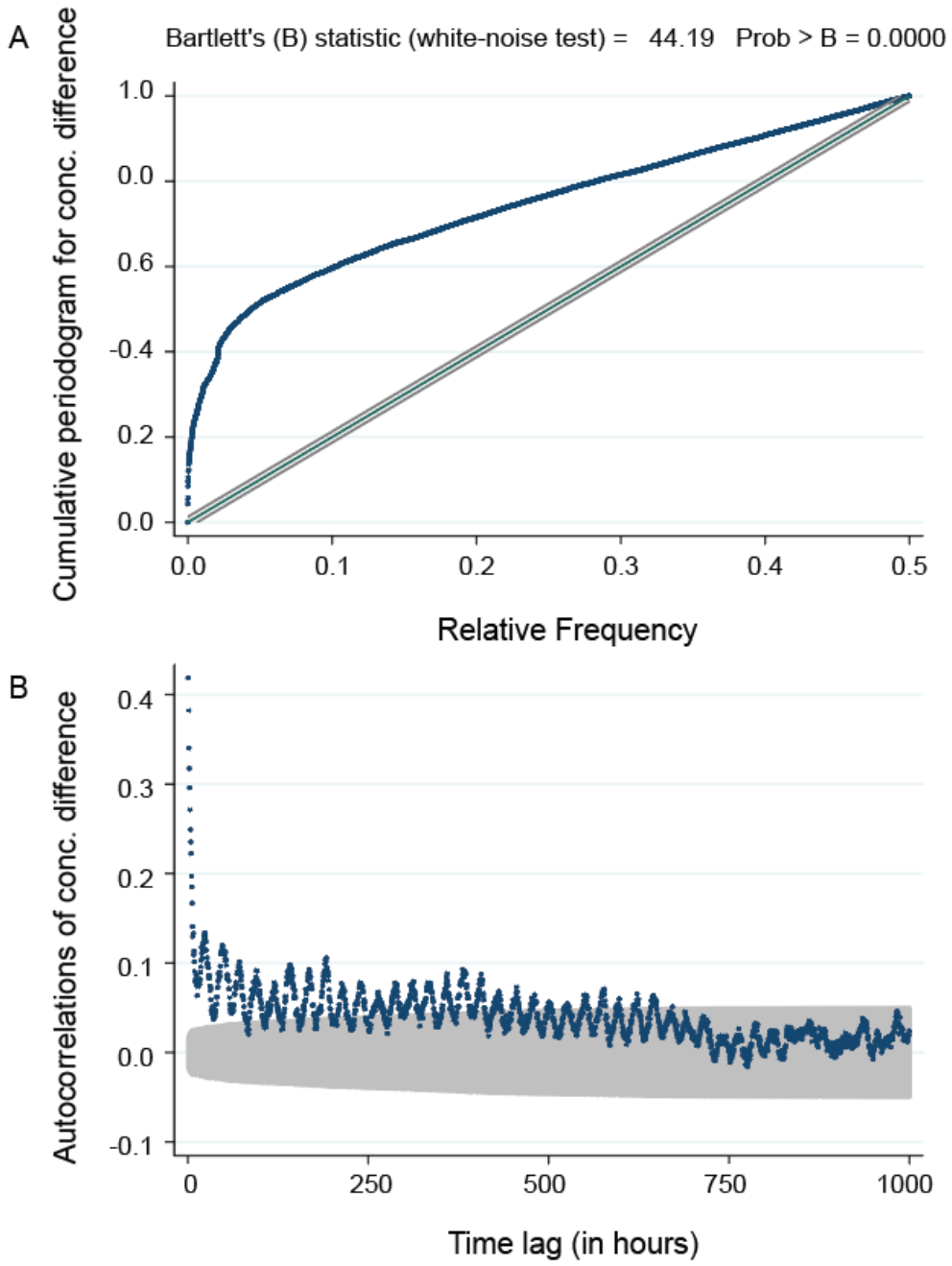

Figure S3A. Cumulative spectral distribution analyses of measured 30-minute GEM concentration differences above the forest canopy. X-axis represent relative frequency based on 22,536 data points. The spectral distribution of a random signal is represented by the three linear gray lines (mean and 95% confidence intervals of a white noise signal). Bartlett statistics shows measurements to be statistically different from a white noise signal ($p < 0.01$). **B.** Autocorrelation (y-axis) of measured GEM concentration differences against time lag of data (x-axis). Strong autocorrelation are visible over short time scales with local peaks in autocorrelations at daily lag intervals. Shaded area represents 95% confidence interval based on Bartlett's formula.

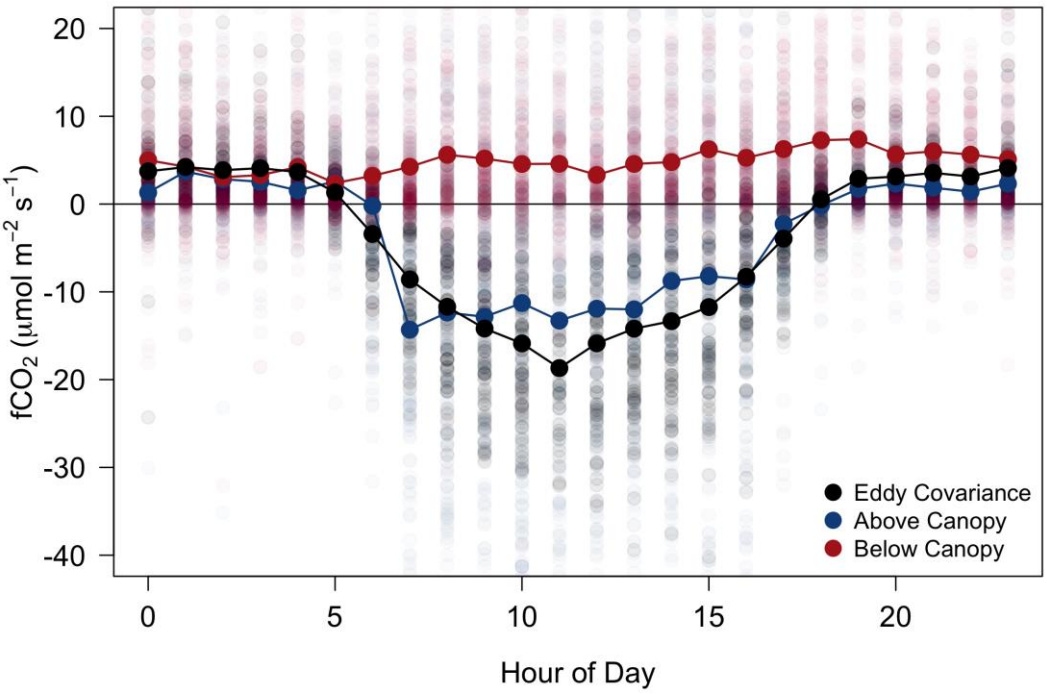

Figure S4. Comparison of ecosystem-level (i.e., above canopy) CO_2 fluxes measured by Eddy Covariance method and flux-gradient method at Harvard forest from June 12 to October 16, 2019. Data points represent hourly averaged data for the full time period. Patterns show high agreement in diel patterns and flux magnitude between the two methods. For below-canopy fluxes, no comparison is available, but data show consistent and expected flux directions driven by underlying forest floor and soil respiration.

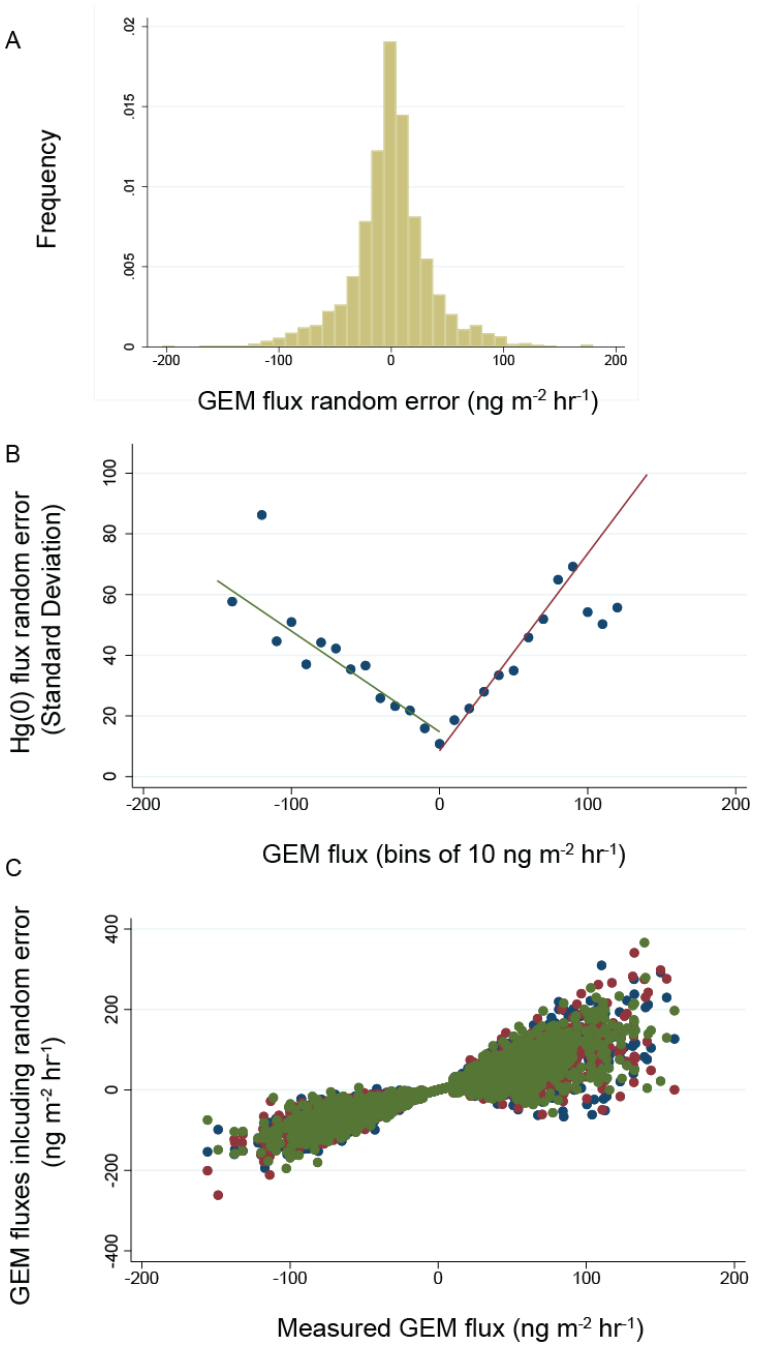

Figure S5. A. Histogram of "daily difference" pairs of GEM observations taken at the same time on two successive days under equivalent environmental conditions. **B.** Relative random errors quantification using scatter plots of mean standard deviations versus flux magnitude (using flux bins of 10 ng m^{-2} hr^{-1}). Regression lines Δstdev/Δmean are a measure of relative standard deviation for each bin of GEM flux measurements. C. Random error assigned to each data point based on a normal frequency distribution (total of 500 data points. Graphs shows scatter plots of the first five randomly generated points against measured GEM fluxes.

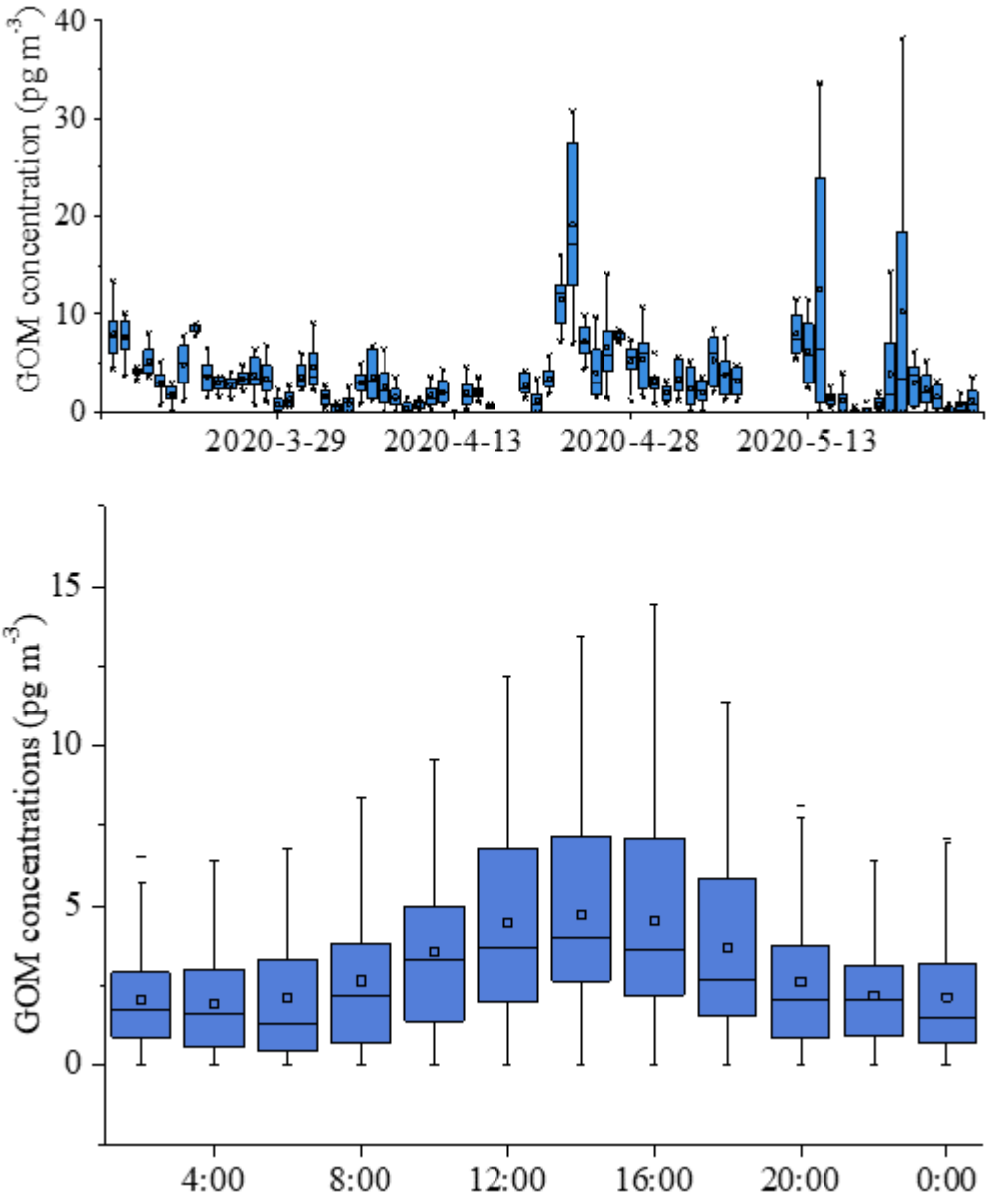

Figure S6. Daily patterns and diel variability of measured GOM concentrations between March 15 to May 27, 2019. GOM concentrations averaged 4.1±5.6 pg m^{-3}. Using a reported deposition velocity of 1.5 cm s^{-1} (14) results in a GOM deposition flux of 0.22±0.30 ng m^{-2} hr^{-1}, or 1.9±2.6 µg m^{-2} yr^{-1} when extrapolated.

Table S1. Summary statistics of daily GEM fluxes at Harvard Forest for the measurement period. Also shown are summary statistics for respective midday GEM fluxes (10 AM to 3 PM) and nighttime fluxes (midnight to 6 AM).

Year	Month	Daily GEM Fluxes (24-hours)					Midday GEM fluxes (10 AM to 3 PM)					Nighttime GEM fluxes (0:00 to 6 AM)				
		Mean	SD	Median	1st quartile	3rd quartile	Mean	SD	Median	1st quartile	3rd quartile	Mean	SD	Median	1st quartile	3rd quartile
2019	5	7.8	8.1	6.5	1.8	10.7	18.9	19.5	17.9	4.7	23.2	1.4	4.0	1.4	-1.8	4.1
2019	6	-1.7	11.6	0.0	-8.5	5.3	0.3	24.3	0.4	-13.2	23.5	-3.4	6.3	-1.7	-4.9	0.6
2019	7	-10.4	8.5	-8.7	-14.0	-4.9	-19.6	16.3	-20.0	-25.3	-9.1	-4.0	5.3	-2.6	-8.3	0.4
2019	8															
2019	9	-11.5	5.2	-12.9	-14.3	-8.4	-22.4	4.9	-24.3	-24.8	-16.8	-6.3	3.9	-6.1	-9.0	-4.3
2019	10	-9.8	5.1	-8.4	-13.5	-5.7	-12.7	19.7	-12.2	-27.2	1.3	-2.9	5.3	-1.2	-7.2	0.5
2019	11	-9.8	7.1	-10.0	-14.2	-2.8	-21.7	15.8	-23.9	-33.7	-7.4	-1.5	6.3	0.0	-3.5	1.6
2019	12	4.2	13.6	2.3	-3.0	8.9	6.0	20.7	7.6	-2.5	13.2	6.2	15.3	2.3	-1.7	6.9
2020	1	9.7	9.7	8.5	2.9	14.2	15.3	19.0	11.1	1.7	25.8	6.4	8.9	4.8	1.1	11.6
2020	2	-0.1	9.5	1.1	-8.5	8.1	2.2	29.1	5.1	-18.6	21.0	-0.8	3.6	-0.1	-4.5	2.1
2020	3	-0.3	9.1	1.7	-6.6	3.8	5.2	24.1	2.4	-14.7	15.9	-3.7	5.5	-3.1	-6.9	0.8
2020	4	2.1	12.7	2.0	-3.8	9.5	12.0	31.5	10.0	-13.9	36.5	-3.7	5.6	-3.0	-6.4	-0.1
2020	5	1.9	16.4	0.4	-9.8	11.0	-9.5	34.5	-12.9	-39.5	23.7	2.0	6.0	0.5	-1.5	4.5
2020	6	-5.6	10.9	-4.9	-13.8	2.4	-14.7	22.8	-19.6	-26.6	-1.5	-3.0	6.4	-1.9	-6.0	0.2
2020	7	-9.1	11.4	-9.3	-17.3	-4.3	-18.3	21.6	-15.1	-33.1	-9.8	-3.1	3.9	-3.0	-4.5	-1.3
2020	8	-18.0	6.0	-17.5	-24.6	-13.7	-27.8	16.7	-26.8	-38.9	-18.8	-6.3	5.9	-3.4	-13.3	-1.8

GEM fluxes in units of ng GEM m^{-2} hr^{-1}, positive fluxes are emissions, negative fluxes are deposition

References

1. Agnan Y, Le Dantec T, Moore CW, Edwards GC, & Obrist D (2016) New constraints on terrestrial surface atmosphere fluxes of gaseous elemental mercury using a global database. *Environ Sci Technol* 50(2):507-524.
2. Obrist D*, et al.* (2017) Tundra uptake of atmospheric elemental mercury drives arctic mercury pollution. *Nature* 547:201-2014.
3. Commane R*, et al.* (2015) Seasonal fluxes of carbonyl sulfide in a midlatitude forest. *P Natl Acad Sci USA* 112(46):14162-14167.
4. Meredith LK*, et al.* (2014) Ecosystem fluxes of hydrogen: a comparison of flux-gradient methods. *Atmospheric Measurement Techniques* (9).
5. Goldstein AH, Daube BC, Munger JW, & Wofsy SC (1995) Automated in-situ monitoring of atmospheric non-methane hydrocarbon concentrations and gradients. *J Atmos Chem* 21(1):43-59.
6. Goldstein AH, Fan SM, Goulden ML, Munger JW, & Wofsy SC (1996) Emissions of ethene, propene, and 1-butene by a midlatitude forest. *Journal of Geophysical Research: Atmospheres* 101(D4):9149-9157.
7. Goldstein AH, Goulden ML, Munger JW, Wofsy SC, & Geron C (1998) Seasonal course of isoprene emissions from a midlatitude deciduous forest. *Journal of Geophysical Research: Atmospheres* 103(D23):31045-31056.
8. McKinney KA, Lee BH, Vasta A, Pho TV, & Munger JW (2011) Emissions of isoprenoids and oxygenated biogenic volatile organic compounds from a New England mixed forest. *Atmos. Chem. Phys.* 11(10):4807-4831.
9. Muller JBA*, et al.* (2009) Comparison of ozone fluxes over grassland by gradient and eddy covariance technique. *Atmospheric Science Letters* 10(3):164-169.
10. Meredith LK*, et al.* (2014) Ecosystem fluxes of hydrogen: a comparison of flux-gradient methods. *Atmos. Meas. Tech.* 7(9):2787-2805.
11. Moore KE*, et al.* (1996) Seasonal Variation in Radiative and Turbulent Exchange at a Deciduous Forest in Central Massachusetts. *Journal of Applied Meteorology (1988-2005)* 35(1):122-134.
12. Hollinger DY & Richardson AD (2005) Uncertainty in eddy covariance measurements and its application to physiological models. *Tree Physiol* 25(7):873-885.
13. Richardson AD*, et al.* (2006) A multi-site analysis of random error in tower-based measurements of carbon and energy fluxes. *Agr Forest Meteorol* 136(1):1-18.
14. Zhang LM, Wright LP, & Blanchard P (2009) A review of current knowledge concerning dry deposition of atmospheric mercury. *Atmos Environ* 43(37):5853-5864.